DOI 10.1007/s10527-023-10233-7
Biomedical Engineering, Vol. 56, No. 5, January, 2023, pp. 345–352. Translated from Meditsinskaya Tekhnika, Vol. 56, No. 5, Spt.–Oct., 2022, pp. 37–41
Original article submitted September 30, 2022

Constructional Features of a Multielectrode Electrocardiology Screening System

M. N. Kramm,[1,*] O. N. Bodin,[2] A. Yu. Bodin,[3] T. L. N. Truong,[3] and G. V. Zhikhareva[3]

The challenges of constructing a noninvasive screening system for electrocardiodiagnostics, focused on visualization of electric potential maps on the surface of the epicardium, is addressed. A functional diagram of a module for recording multiple-lead electrocardiosignals is proposed, the essential component of which is a vest (in several standard sizes) worn by the subject and carrying pre-installed electrodes. Results obtained from experimental verification of the operation of the recording module are presented. The issues of computer processing of electrocardiosignals were addressed and led to the ability to obtain 2D maps of the electric potential on a spherical quasi-epicardium, these 2D maps changing synchronously with changes in the position of the time marker on electrocardiograms familiar to cardiologists.

Introduction

Cardiovascular disease (CVD) is an major problem in modern healthcare which, according to the World Health Organization, stably takes first place throughout the world in terms of mortality due to disease. The main ways to reduce mortality from CVD are prevention and timely diagnosis. Preventive examination (screening) of the population takes first place in this. The relevance of electrocardiological screening is increasing in the struggle against the COVID-19 epidemic and its consequences in the form of various comorbid complications. Increasing the reliability and efficiency of the diagnosis of heart diseases by electrocardiological screening is therefore an important social task.

In general, classical ECG methods are very important for diagnosis [1]. However, these methods give an incomplete idea of the spatio-temporal dynamics of the processes of excitation and repolarization of cardiac muscle, which is important for locating areas with anomalies in these dynamics. The sensitivity of these diagnostic methods for coronary heart disease is also low (about 65–70% even for stress tests) [2, 3]. Important methods of high-resolution electrocardiography [4], dispersion mapping [5], and torso surface mapping of potentials [6] are known. However, an interfering factor in determining the locations and estimating the sizes of pathological areas of myocardium comes from the effects of attenuation of harmonics in the spectrum of the spatial distribution of the electric potential during propagation from the myocardial area to the surface of the torso [7]. These points are confirmed by comparing the torso surface potential map (TSPM) and the epicardial surface potential map (ESPM), shown in Fig. 1 for the same case; maps were obtained by mathematical modeling.

Important methods for mapping the potential on the heart surface based on solution of the inverse electrocardiography problem [8–10] are intended for preoperative examination in cardiology centers. These are not focused on conducting screening examinations because of the significant hardware and organizational costs, as well as the increase in examination duration associated with the use of X-ray, tomography, or MRI reconstruction of the surfaces of the torso and epicardium and the use of systems for collecting multichannel electrocardiosignals from up to 224 electrodes.

Thus, on the one hand, classical ECG methods are convenient for screening examinations but not sufficiently informative for spatial representation of the electrical activity of the heart (EAH). On the other hand, existing methods of EAH mapping on the heart surface, based on solution of the inverse electrocardiography problem, are quite complicated for the purposes of electrocardiological screening and require significant hardware and time resources that do not allow screening for the prevention

[1]Moscow Energy Institute National Research University, Moscow; E-mail: Krammmn@mpei.ru
[2]Department of Technical Quality Control, Penza State Technology University, Penza.
[3]Department of Basic Radio Technology, Moscow Energy Institute National Research University, Moscow.
[*]To whom correspondence should be addressed.

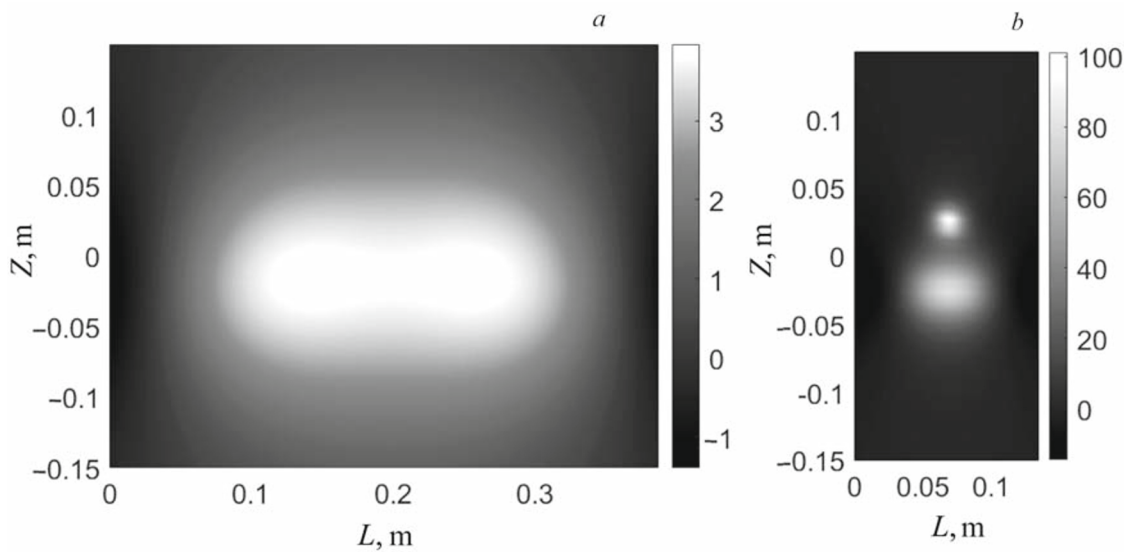

Fig. 1. TSPM and ESPM for the same case: a) TSPM, coordinate *L* changes along the perimeter of the torso model; b) ESPM, coordinate *L* changes along the perimeter of the quasi-epicardium.

of CVD associated with the presence of myocardial areas with the excitation abnormalities typical of ischemic and arrhythmogenic conditions.

The aim of our work was to build a multielectrode electrocardiological screening system focused on visualization of electric potential maps on the epicardial surface with the aim of increasing the reliability of electrocardiodiagnostic screening systems [11].

Materials and Methods

The authors developed a method and system for recording electrocardiosignals (ECS) from multiple leads [12]. The multiple-lead ECS recording system contains a series-connected module for recording ECS from multiple leads, which consists of an electrode assembly, a data transmission unit, and a data acquisition, processing, and storage module.

When recording ECS, 50–100 unipolar electrodes are distributed evenly on the front, back, and side surfaces of the torso. A significant difficulty in screening is the time taken to install the large number of electrodes and the need to install them at the correct points on the torso surface (the electrode coordinates are used in reconstructing ESPM). To overcome this difficulty, we proposed an ECS recording unit [12] consisting of a vest with pre-installed electrodes worn by the subject, lead connecting wires, and connectors (Fig. 2).

Use of the vest significantly reduces the electrode installation time. Differences in subjects' torso sizes are taken into account by the elasticity of the vest material, as well as the use of vests of several standard sizes. The Small size fits a torso with a cross section perimeter of L = 70–90 cm, the Medium size fits L = 90–110 cm, and the Large size fits L = 110–130 cm [4].

In order to record electrocardiosignals from multiple leads (64 in our case), the authors proposed a block diagram

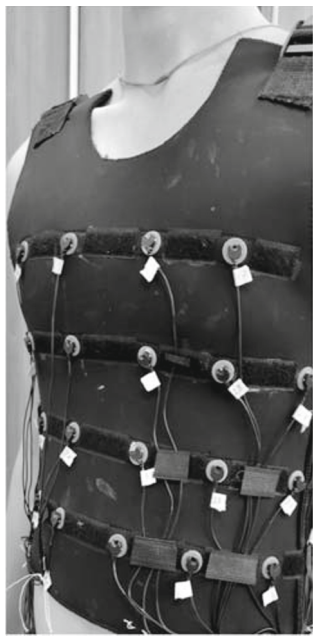

Fig. 2. Vest with pre-installed electrodes.

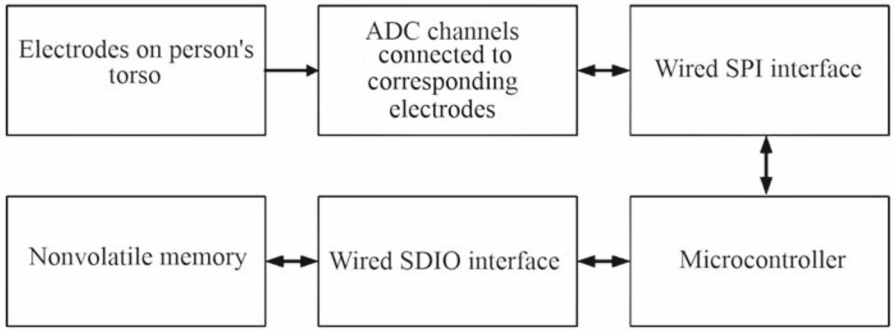

Fig. 3. Block diagram of module for multiple-lead ECS recording.

of the multiple lead ECS recording module (Fig. 3). This shows "expanded" blocks for the recording module for multiple ECS leads. The first block contains the vest with electrodes distributed evenly in various locations on the person's torso [12]. The second block consists of eight-channel analog-to-digital converters (ADC) connected to the corresponding electrodes. The third block is a wired interface providing communication between the ADC and the microcontroller (MCU). The fourth block is the microcontroller responsible for recording and sampling ECS from multiple leads at the required frequency and storing the results in nonvolatile memory. The fifth block is a wired interface providing communication between the microcontroller and the nonvolatile memory. The sixth block is the nonvolatile memory (SD Card). The sampling frequency for each ECS was 1 kHz. A 24-bit (3 bytes) binary code is generated at the ADC output, the value corresponding to the digitized level of the ECS recorded at the time of recording.

Computer processing of ECS recorded in multiple leads includes the following steps: 1) pre-processing of ECS, including correction of baseline drift and noise filtration in the upper and lower frequencies; 2) creation of grids of boundary elements on the torso and epicardium surface; surface element areas should be similar for each surface; 3) interpolation of the measured electrode potentials onto a fine grid on the torso surface; 4) reconstruction of the distribution of the potentials of the fine grid on the epicardial surface elements; 5) visualization of a 2D or 3D potential map on the epicardial surface (ESPM). It is fundamental that steps 3–5 are repeated for the time points corresponding to the selected segments of the cardiac cycle (P-wave, QRS complex, ST–T segment, T-wave).

In accordance with Green's theorem [7] and taking into account the condition of electrical isolation of the torso (no outflowing currents) for the observation points located on the epicardial or torso surface, a system of linear algebraic equations (SLAE) was obtained relating the potentials on the epicardial surface and their derivatives in the direction normal to this surface with the known potentials on the torso surface at the current time point. The SLAE contains matrixes H^{hh}, H^{bh}, H^{hb}, H^{bb}, G^{hh} and G^{hb}, which are determined by the geometry of the torso and epicardial surfaces. Optionally selected variants of such surfaces are provided by torso surface models in the form of an elliptical cylinder. A realistic triangulation model of the epicardial surface is used and, for convenience in 2D visualization of the planar transform of the heart surface, a spherical model of the quasi-epicardium (a sphere circumscribed around the surface of the epicardium) is used.

In the course of the reconstruction of the ESPM for each time point of the selected cardiac cycle interval, the SLAE is solved iteratively using the Seidel method, iterations starting with the conversion of the better posed matrixes. For the *k*-th iteration

$$\varphi_k^h = (H^{hh})^{-1}(G^{hh} g_{k-1}^h - H^{bh}\varphi^b) ,$$

$$g_k^h = (G^{hb})^{-1}(H^{hb}\varphi_k^h + H^{bb}\varphi^b) , \qquad (1)$$

and $\phi_1{}^h = -(H^{hh})^{-1}(H^{bh}\phi^b)$ for the first iteration. Before running iterative procedure (1), the conversion of the ill-posed matrix G^{hb} is regularized using the truncated singular value decomposition (TSVD) method [13]. In this case, the singular value decomposition of this matrix $G^{hb} = URV^T$ is used, where U and V are the orthogonal matrices of sizes $N_b \times N_b$ and $N_h \times N_h$, respectively; R = diag(ρ_1, ρ_2, …, ρ_M) is a rectangular diagonal matrix of size $N_b \times N_h$ containing singular values on the diagonal $\rho = (\rho_1, \rho_2, \ldots, \rho_M)$, where M = min($N_h$, N_b); $\rho_1 \geq \rho_2 \geq, \ldots \geq \rho_M \geq 0$. As instability on conversion of matrixes is associated with the contribution of small singular numbers, introduction of a filter for small singular numbers is proposed, with a transfer coefficient of

$$K(\rho) = \frac{1}{1 + \left(\frac{\rho_{cb}}{\rho}\right)^2 \frac{1 - K_{gr}}{K_{gr}}},$$

where ρ_{cb} is the first singular value, counting from the beginning of the vector ρ, for which the condition $(\rho_1/\rho_i) > C_b$ is satisfied (C_b is a parameter specifying the range of singular values taken into account) [14]; $K_{gr}(\rho_{sv}) = 1/2^{1/2}$. The generally accepted regularization coefficient is $\alpha = \rho_{cb}^2(1 - K_{gr})/K_{gr}$. The regularized pseudo-inverse matrix is then

$$(\tilde{G}^{hb})^{-1} = V\tilde{R}^{+}U^{T},$$

where

$$\tilde{R}^{+} = \text{diag}\left[K(\rho_1)\rho_1^{-1},\ K(\rho_2)\rho_2^{-1},\ ...,\ K(\rho_M)\rho_M^{-1}\right].$$

A convenient visualization method is provided by 2D electrical potential mapping on a planar transforms of the surface of a spherical quasi-epicardium circumscribed around the surface of the heart [15, 16]. The correspondence of the chambers of the heart and areas on the planar transform of the surface of the quasi-epicardium is shown in Fig. 4.

The potential on the surface of the quasi-epicardium is reconstructed using a grid with divisions of the elevation angle and azimuth such that the elements of the sphere surface are equal in area. This ensures uniform digitization and the best posing of the SLAE matrixes in the reconstruction of the potential map [13]. At the same time, for the purpose of visualization it is desirable that distances between points on the planar transform are equal when the lengths of the arcs between the points of the surface of the sphere are equal. This allows the sizes of regions of electrical activity to be estimated directly from the 2D map. Figure 5 shows the locations of the points of the proposed grid on the surface of the planar transform of the quasi-epicardium together with the reference meridians. The central meridian passes through the centers of the left atrium and left ventricle.

RESULTS

Verification of the Operating Speed of the Multiple-Lead ECS Recording Module

The response size from one ADC channel is 3 bytes; it follows from this that the size of the response from the entire channel group (64 channels) is 192 bytes. The SPI does not use start or stop bits, so there is no "lost" signal

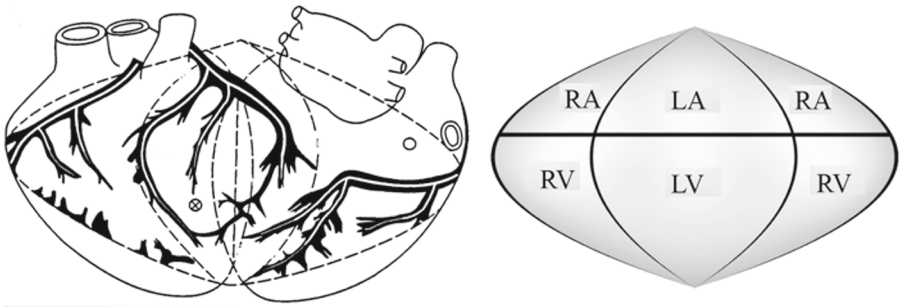

Fig. 4. Planar transform of the surface of the quasi-epicardium [8]; RA and LA — right and left atria; RV and LV — right and left ventricles.

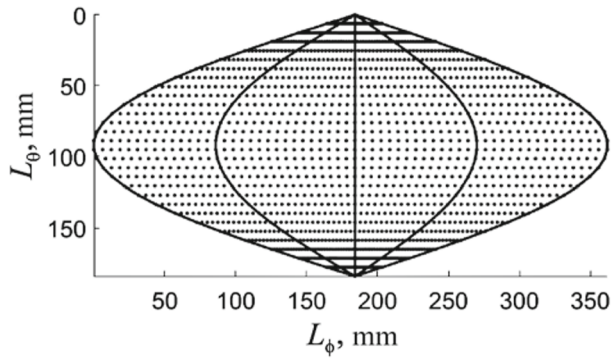

Fig. 5. Grid points on a planar transform of the epicardial surface.

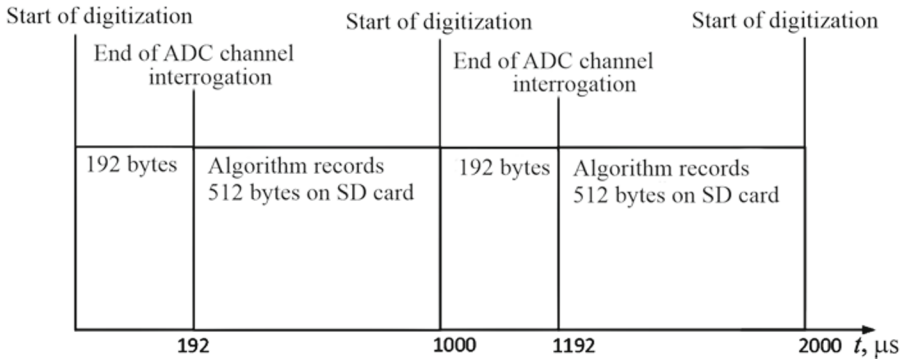

Fig. 6. Timing diagram for one interrogation cycle of multiple ECS leads.

time. With an effective SPI bus operating frequency of 8 MHz, we get a bit rate of 8 Mbit/s, while polling the channel group will take

$$t_{\text{cardiogroup}} = t_{\text{bit}} N_b N_{\text{channel}},$$

where t_{bit} = 0.125 μs is the time taken to send one bit; N_b = 24 is the number of bits in the response to the request to read one sample of the ECS channel; N_{channel} = 64 is number of channels. As a result, we get $t_{\text{cardiogroup}}$ = 192 μs. Figure 6 shows the timing diagram for one polling cycle.

The values obtained for the electrode potentials must be constantly transferred from the internal memory of the microcontroller (192 kB) to the external non-volatile memory. For recording the results on an SD card without losses, the required recording time must not exceed

$$t_{\text{write\_max}} = (1/f_{\text{sample}}) - t_{\text{cardiogroup}}, \qquad (2)$$

where f_{sample} is the sample rate. Based on Eq. (2), we get $t_{\text{write\_max}}$ = 808 μs i.e., the maximum time for data to be written to the SD card.

Data are recorded on the SD card in packets of 512 bytes (512 is the recommended packet length for recording to the SD Card at which the maximum recording speed is achieved), which takes about 700 μsec for a packet (see Fig. 6).

We have implemented a prototype device for recording multiple ECS leads and have proposed an algorithm for the microprocessor based on the above calculations and timing diagrams. Figure 7 shows the timing diagram for recording 64-lead electrocardiogram readings on the SD card. Since write packet length is greater than the channel group length (192 bytes), the remaining 320 bytes in the packet are packed with zeros. The results are presented on the monitor screen of a logic analyzer connected to the device in the test signal mode. Here:

- Channel 1 is the channel connected to the microcontroller port, and its state changes when recording on the SD card starts: Low = no recording, High = recording is active;
- Channel 2 is a channel connected to the SPI_MOSI data line, through which the microcontroller sends requests to read the electrode potentials;
- Channel 3 is a channel connected to the SPI_MISO line, through which the ADC sends responses to the request to read electrode potentials:
- Channel 4 is a channel connected to the SPI_CLK clock bus;
- Channel 5 is a channel connected to the SPI Chip Select — ADC selection.

Figure 7 visually confirms the adequate implementation of the proposed high-speed time parameters for the process of polling 64 ECS channels at a sampling rate of 1 kHz and recording ECS readings on an SD card.

Visualization of the Electrical Activity of the Heart

Figure 8 shows results obtained by visualization of cardiac electrical activity with processing of real ECS using the method described above. This shows the mode in which the pseudo-color scale is determined dynamically by the maximum and minimum values of the potential for the 2D map at the current time point. This clearly shows the boundaries of regions with different electrical activity.

ECS were recorded and processed from unipolar electrodes distributed uniformly over the torso (chest and back). For clarity, the upper part of Fig. 8 shows the electrocardiogram of limb lead II, which is familiar to cardiologists, while the lower part shows 2D maps of the electrical potential on a planar transform of the quasi-epicardium surface for the time points at the centers of the P-wave (map 1), QRS complex (map 2) and T-wave (map 3).

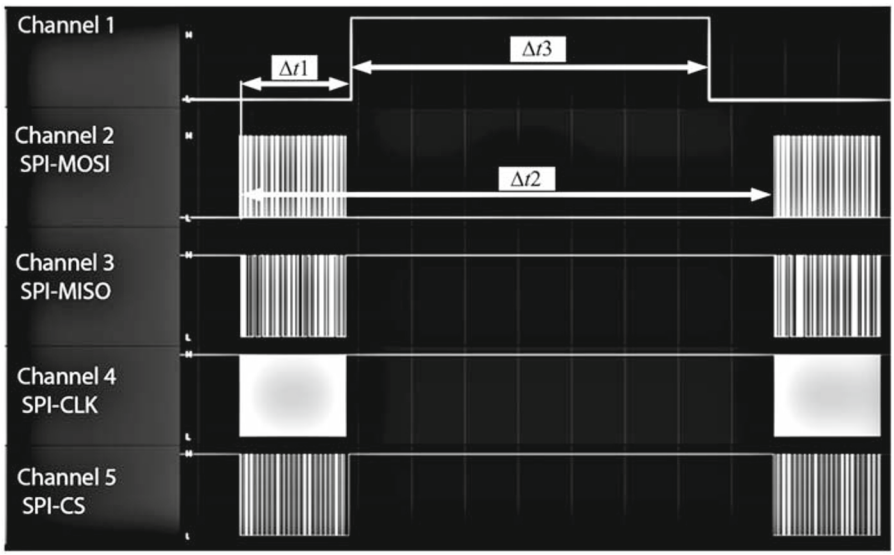

Fig. 7. Test signal recording mode on the logic analyzer screen: Δt_1 = 211 μs; Δt_2 = 1000 μs; Δt_3 = 658 μs.

The corresponding time points are indicated by markers (bold dots) on the upper ECS. Dynamic representation of the EAH in interactive mode is provided by the option to displace the time point within the waves using sliders 4 (P-wave), 5 (QRS-complex), and 6 (T-wave). As the slider moves along the timeline, the corresponding 2D map is updated and the time marker on the electrocardiogram is synchronously shifted. The time step is a selectable option, with a default of 4 msec. It is essential that the computational reconstruction of the electrical potential maps on the quasi-epicardium is carried out before the visualization phase, i.e., at the stage of processing the multiple-lead ECS. The electric potential level is displayed in Fig. 8 on a gray scale placed vertically beside each 2D map (in fact, a scale of pseudo-colors from red to blue is used, which takes into account the sign of the potential and more clearly highlights small areas).

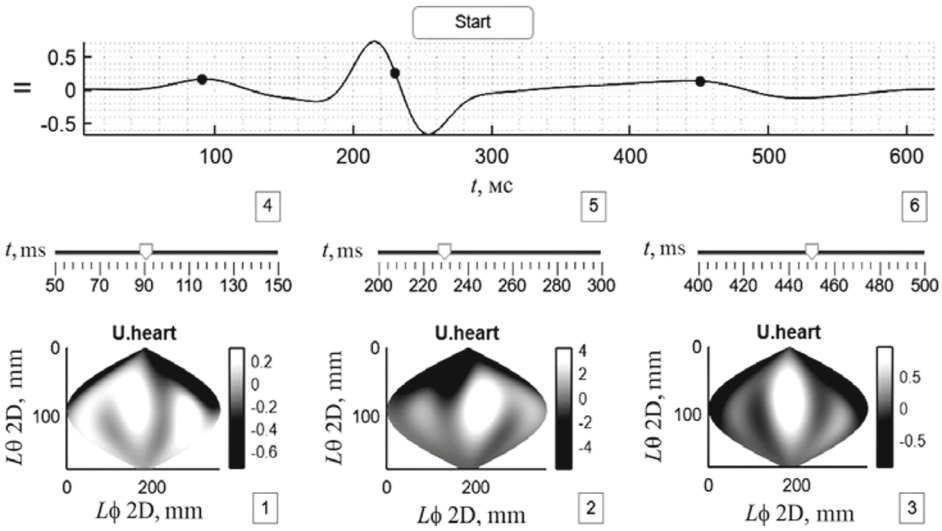

Fig. 8. Visualization of EAH on planar transform of the quasi-epicardium surface.

Conclusions

The scheme of the multiple-lead ECS recording module presented here is intended for the reconstruction and visualization of maps of the electrical activity of the heart on the surface of the epicardium. The estimates of the time intervals during the ADC interrogation and recording data are focused on the recording 64 channels at a sampling rate of 1 kHz per channel. The results obtained from experimental verification of the performance of the ECS recording module confirm the correctness of the calculations obtained and the absence of information loss when recording to non-volatile memory in real time.

Reconstruction of the electric potential distribution map on the surface of the quasi-epicardium makes it possible to detect size inhomogeneities of the order of 2–3 cm, which is impossible in the case of potential maps constructed on the torso surface. The proposed temporal synchronization of 2D potential maps on the surface of the heart and the electrocardiogram, which is familiar to cardiologists, contributes to visualization of the dynamics of cardiac electrical activity through the cardiac cycle. Another advantage of the 2D potential map is the ability to observe the temporal dynamics of electrical activity in all areas of the myocardium without an additional change in perspective.

Further development of the noninvasive electrocardiological screening system will involve validation of the system by comparing the results obtained with transesophageal ECG data. Also relevant are the issues of optimizing the program code and increasing the detail of the ESPM maps, with an increase in the number of electrodes in the cardiac vest up to 80–100.

Overall, the approach proposed here is focused on providing the cardiologist with visual information during screening examinations, displaying the movement of areas of electrical activity of the heart on the surface surrounding the epicardium as it changes dynamically in time. This visualization mode, synchronized with changes in classical ECG signals, allows potential maps in the epicardial region to be linked with specific phases of the cardiac cycle.

REFERENCES

1. Macfarlane, P. W., Van Oosterom, A., Pahlm, O., Kligfield, P., Janse, M., and Camm, J., Comprehensive Electrocardiology, Springer, London (2011), 2nd edition.
2. Syrkin, A. L., Aksel'rod, A. S., Novikova, I. A., Poltavskaya, M. G., Sedov, V. P., Chomakhidze, P. Sh., and Pasha, S. P., Guidelines for the Functional Diagnosis of Heart Diseases [in Russian], A. L. Syrkin (ed.), Gold Standard, Moscow (2009).
3. Gibbons, R. J., et al., "ACC/AHA 2002 guideline update for exercise testing: Summary article: A report of the American College of Cardiology/American Heart Association Task Force on Practice Guidelines (Committee to Update the 1997 Exercise Testing Guidelines)," J. Am. Coll. Cardiol., **40**, No. 8, 1531–1540 (2002).
4. Grachev, S. V., Ivanov, G. G., and Syrkin, A. L., New Methods in Electrocardiography [in Russian], Tekhnosfera, Moscow (2007).
5. Ivanov, G. G. and Sula, A. S., Dispersion EEG Mapping: Theoretical Grounds and Clinical Practice [in Russian], Tekhnosfera, Moscow (2009).
6. Polyakova, I. P., "Surface EEG mapping as a method for the diagnosis of heart rhythm abnormalities, Ch. 6, in: Noninvasive Diagnostics in Clinical Arrhythmology. A Monograph [in Russian], Meditsina, Moscow 1(2009), pp. 157–175.
7. Titomir, L. I. and Kneppo, P., Mathematical Modeling of the Bioelectric Generator of the Heart [in Russian], Nauka, Fizmatlit, Moscow (1999).
8. Rudy, Y., "Noninvasive electrocardiographic imaging of arrhythmogenic substrates in humans," Circ. Res., **112**, 863–874 (2013).
9. Bokeriya, L. A., Revishvili, F. Sh., Kalinin, F. V., Kalinin, V. V., Lyakhina, O. S., and Fetisova, E. A., "A software and hardware system for the noninvasive electrophysiological examination of the heart based on solution of the inverse problem of electrocardiography," Meditsinsk. Tekhn., No. 6, 1–7 (2009).
10. Potyagaylo, D., Cortes, E. G., Schulze, W. H. W., and Dössel, O., "Binary optimization for source localization in the inverse problem of ECG," Med. Biol. Eng. Comput., **52**, 717–728 (2014).
11. Bodin, O. N., Kramm, M. N., Ozhikenov, K. A., and Rakhmatullov, F. K., Current Noninvasive Cardiodiagnostic Technologies, TOO Lantar Trade, Almaty (2021).
12. Bodin, O. N., Kramm, M. N., Bodin, A. Yu., Rakhmatullov, R. F., Rakhmatullov, F. K., Safronov, M. I., Fedorenko, A. I., and Chernikov, A. I., A Method and Device for Recording Multiple Electrocardiosignal Leads [in Russian], Russian Federation Patent No. 2764498 RF; published January 17, 2022; Byul. No. 2.
13. Leonov, A. S., Solution of Ill-Posed Inverse Problems, Outline of Theories, Practical Algorithms and Demonstrations in MATLAB [in Russian], Librokom, Moscow (2010).
14. Kramm, M. N., "Analysis of the effects of the selection of the number of electrodes on the results of reconstructions of the electric potential distribution on the surface of the epicardium," Modeli, Sistemy, Seti v Ékonomike, Tekhnike, Prirode i Obshchestve, No. 1 (33), 78–85 (2020).

15. Titomir, L. I., Trunov, V. G., and Aidu, É. A. I., Noninvasive Electrocardiotopography [in Russian], Nauka, Moscow (2003).
16. Zhikhareva, G. V., Kramm, M. N., Bodin, O. N., Seepold, R., Chernikov, A. I., Kupriyanova, Y. A., and Zhuravleva, N. A., "Reconstruction of equivalent electrical sources on heart surface," in: Proceedings of the 6th International Work–Conference, IWBBIO 2018, Granada, Spain, April 25–27, 2018, Part I.